CHAPTER V
EFFECTS OF BALL-MILLING TIME ON THE DECOMPOSITION OF THE $LiBH_4$ AND MgH_2 MIXTURE

5.1 Abstract

Effects of milling time on the hydrogen desorption/absorption behaviors of a 2:1 molar ratio of $LiBH_4$ and MgH_2 mixture were investigated. The milling time was varied from 1 to 10 h. The hydrogen desorption/absorption was carried out in a Seivert's type apparatus. The hydrogen desorption was performed from 25 to 500°C by using a heating rate of 2°C min^{-1} under 0.1 MPa H_2. The sample was compressed under 8.5 MPa H_2 at 350°C for the hydrogen absorption. The sample characterization was accomplished through XRD and DSC. In the first desorption, the samples milled with different ball-milling times decomposed hydrogen in three steps with the same starting temperature of 50°C, and the ball-milling time of 5 h exhibited the highest hydrogen desorption capacity of 9.2 wt%. In the subsequent hydrogen desorption, all samples released hydrogen only two steps at different starting desorption temperatures. The milling time of 10 h resulted in the lowest hydrogen desorption temperature of 340°C and the highest reversible hydrogen capacity of 4.2 wt% in the forth desorption.

5.2 Introduction

Solid state hydrides such as alkaline metal and alkaline earth metal borohydrides have become particularly attractive for hydrogen storage because they contain high gravimetric and volumetric hydrogen density not to mention their reversibility property. However, their thermodynamics and kinetics are too stable for practical mobile applications [1,2]. It has been confirmed that the thermodynamic properties (e.g. reaction enthalpy) can be improved by alloying and/or reacting the borohydrides with a metal and/or a metal hydride through ball milling to change the reaction pathway so called reactive hydride composite (RHC) [3-5]. The addition of

an appropriate catalyst can also lower the activation energy [6], while the milling technique can reduce the particle size of the hydrides together with the diffusion distance for hydrogen resulting in faster reaction kinetics [7-9].

One of the most attractive borohydrides is $LiBH_4$ because it provides high gravimetric hydrogen density of 18.5 wt%. Without any catalyst, the hydrogen desorption starts at a temperature higher than 400°C and the reaction is irreversible [10]. The hydrogen desorption and absorption properties of $LiBH_4$, such as hydrogen desorption temperature, hydrogen storage capacity, reaction kinetics, and reversibility, have been extensively studied. In 2003, Züttel et al. [11,12] doped $LiBH_4$ with 75 wt% SiO_2 catalyst. The result showed that the hydrogen desorption started at 200°C with 9 wt% total hydrogen capacity. Au and co-workers [13-15] reduced the hydrogen desorption temperature and improved the reversibility by adding various types of metal oxide and metal chloride catalysts. They reported that the addition of 25 wt% TiO_2 to $LiBH_4$ could desorb 9.0 wt% H_2 in a temperature range of 100 to 600°C and absorb 8.0 wt% H_2 at 600°C and 7.0 MPa H_2. However, the reversible hydrogen storage capacity of $LiBH_4$ gradually decreased due to the loss of boron during the hydrogen desorption. In the case of metal chloride catalysts, 1-2 mol% of $MgCl_2$ and $TiCl_3$ were added to $LiBH_4$. It released 5.0 wt% H_2 from 60 to 450°C and absorbed 4.5 wt% H_2 at 600°C and 7.0 MPa H_2. Vajo et al. [16], who first attempted to lower the hydrogen desorption temperature of $LiBH_4$ by using the RHC concept, mixed LiH with MgB_2 (a 2:1 molar ratio) including 2-3 mol% $TiCl_3$. The result showed that the mixture reversibly stored about 8-10 wt% H_2 with two-step hydrogen desorption at 270 and 380°C for the first and second step, respectively. It was claimed that the RHC not only lowers the hydrogen desorption temperature but also contributes to the reversibility via the formation of MgB_2 during the hydrogen desorption. A 1:2 mass ratio of $LiBH_4$ and MgH_2 was added with 16 wt% Nb_2O_5 [17]. The sample released hydrogen below 400°C with 6-8 wt% H_2, and the hydrogen absorption of 5-6 wt% was achieved at 400°C and 1.9 MPa H_2.

Ball-milling time and speed have been reported to affect the hydrogen desorption/absorption behaviors of hydrides. The increase in the ball-milling time and speed can increase the surface area and reduce the particle and crystallite size of

hydrides. In addition, it also increases the lattice microstrain and defects on the surface and in the interior of the hydride structure. The induced microstrain reduces the hysteresis of hydrogen absorption and desorption, while the induced lattice defects provide many sites with low activation energy of diffusion [18,19]. This resulted in the lower hydrogen desorption temperature, higher amount of released hydrogen as well as faster hydrogen desorption/absorption kinetics. However, prolonging the ball-milling time leads to the agglomeration of the small hydride particles, which, in turn, increases the particle size, decreases the surface area, and ultimately, increases the desorption temperature as well as decreases the desorption capacity [20].

Wan et al. [21] mixed MgB_2 with LiH in a 1:2 molar ratio without a catalyst by using a high energy ball-milling at a speed of 600 rpm for 3, 24, and 120 h. The results showed that the ability of hydrogen uptake increased with the milling time. The samples started to absorb hydrogen at 160, 175, and 200°C for the ball-milling time of 3, 24, and 120 h, respectively. In addition, the sample with the ball-milling time of 120 h exhibited the highest hydrogen adsorption of 8.3 wt% at 265°C and 9.0 MPa H_2. Fátay et al. [22] investigated the effects of the grain and particle size and the milling duration on the hydrogen desorption temperature and the desorption kinetics or the activation energy of MgH_2 milled with 2 mol% Nb_2O_5 powders. They reported that the grain and particle size reduction decreased the desorption temperature. Without the addition of Nb_2O_5, the size reduction of MgH_2 mainly occurred during the first 120 min of the milling. However, further milling of MgH_2 with Nb_2O_5 only slightly decreased the particle size of MgH_2 because Nb_2O_5 was harder than MgH_2. In terms of the desorption kinetics, it was found that the milling time less than 15 min could decrease the activation energy of MgH_2 + 2 mol% Nb_2O_5. At a longer milling time, the decrease in the activation energy was suppressed due to the penetration of Nb_2O_5 into MgH_2.

In this work, effects of ball-milling time varied from 1 to 10 h at a constant ball-milling speed of 300 rpm on the hydrogen desorption temperature, total hydrogen storage capacity, reversibility, and reaction kinetics of a 2:1 mole ratio of $LiBH_4$ and MgH_2 mixture were studied. XRD characterization was used to investigate the phase transformation of the mixture at different conditions and

evaluate the crystallite size of the hydrides, while differential scanning calorimetry analysis was carried out in order to clarify hydrogen desorption behavior at different ball-milling times.

5.3 Experimental

$LiBH_4$ (95% purity, Acros Organics) and MgH_2 (90% purity, 10% of mainly Mg, Acros Organics) were used as the starting materials without further purification. For the hydride sample preparation, a 2:1 molar ratio of $LiBH_4$ and MgH_2 was milled using a centrifugal ball mill (Retsch ball mill model S100, 250 ml stainless steel vial, stainless steel ball with 1 cm diameter) under nitrogen atmosphere with a ball to powder ratio of 60:1 and a rotation speed of 300 rpm for 1, 5, and 10 h. All sample handlings were performed in a glovebox filled with nitrogen gas to prevent the sample contamination by air and moisture. To evaluate the hydrogen desorption/absorption properties, approximately 0.3 g of the milled sample was transferred to a stainless steel tube reactor containing a K-type thermocouple (Cole Parmer). The reactor was then placed to a Sievert's type apparatus. The hydrogen desorption was carried out under 0.1 MPa H_2 (purity 99.9999%) from 25 to 500°C by using a heating rate of 2°C min^{-1}. The hydrogen absorption was performed under 8.5 MPa H_2 and 350°C for 12 h. Both hydrogen desorption and absorption were repeated in order to investigate the reversibility of the sample. The accumulated pressure released from the sample was measured by a pressure transducer (Cole Parmer, model 68073-68074) and used for calculating the hydrogen desorption capacity.

For the sample characterization, a Rigaku x-ray diffractometer was used for phase transformation identification. The sample was packed on a glass plate covered by a Kapton tape to prevent air and moisture. The measurement was carried out at room temperature over a range of diffraction angles from 20 to 80 with Cu Kα radiation (40 kV, 30 mA). Differential scanning calorimetry was conducted using a Mettler Toledo (DSC 822) in order to study the thermodynamic properties. The

sample was examined over a temperature range of 50 to 500°C with a heating rate 5°C min^{-1} in a nitrogen flow of 40 ml min^{-1}.

5.4 Results and Discussion

The ball-milling time remarkably affects the hydrogen desorption temperature and the total hydrogen desorption capacity as shown in Figs. 5.1-5.3. The figures show the hydrogen desorption profiles in the first to forth desorption of the $LiBH_4/MgH_2$ mixture after ball-milling for 1, 5, and 10 h. Details of the starting hydrogen desorption temperature and the total amount of desorbed hydrogen in each case are also provided in Table 5.1.

In the first desorption (Figs. 5.1-5.3(a)), the decomposition of the samples takes place in three steps regardless of the milling time. The samples release hydrogen at the same starting temperature of 50°C for the first step. The hydrogen desorption capacity in this step or the shoulder [23] is significantly reduced from 3.0 wt% for the sample milled for 1 h to 1.3 and 1.1 wt% for the sample milled for 5 and 10 h, respectively. The reduction may be related to the shift in the phase transformation temperature of $LiBH_4$, which can be further explained using the DSC examination in Fig. 5.4.

From Fig. 5.4, the hydrides milled for 1, 5, and 10 h clearly show at least three endothermic peaks. The first peak at 118-125°C is the phase transformation of $LiBH_4$ from orthorhombic to tetragonal structure, the second peak at 380°C is the melting point of $LiBH_4$, and the other peaks at temperatures higher than 400°C are the decomposition of the $2LiBH_4/MgH_2$ mixture. It is clear that the increase in the ball-milling time affects the phase transformation of $LiBH_4$ and the desorption temperature of the $2LiBH_4/MgH_2$ mixture. The first peak of the DSC pattern observed in the sample milled for 1 h (Fig. 5.4(a)) splits to two small peaks when the sample is milled for 5 and 10 h (Fig. 5.4(b) and (c)). In addition, the peak is shifted to a higher temperature from 118°C (Fig. 5.4(a)) to 125°C (Fig. 5.4(b) and (c)). This implies that the longer the milling time, the higher the phase transformation

temperature of $LiBH_4$, which may decrease the amount of desorbed hydrogen at the shoulder.

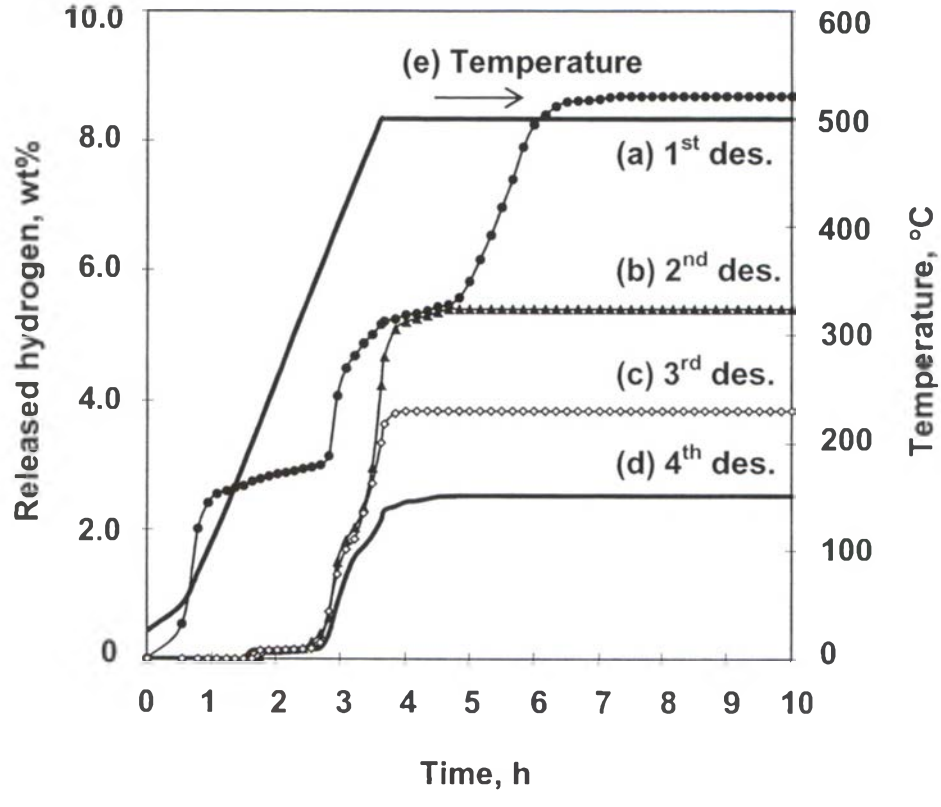

Figure 5.1 Hydrogen desorption profiles of the $LiBH_4/MgH_2$ mixture after ball-milling for 1 h (a) first, (b) second, (c) third, (d) forth hydrogen desorption, and (e) temperature.

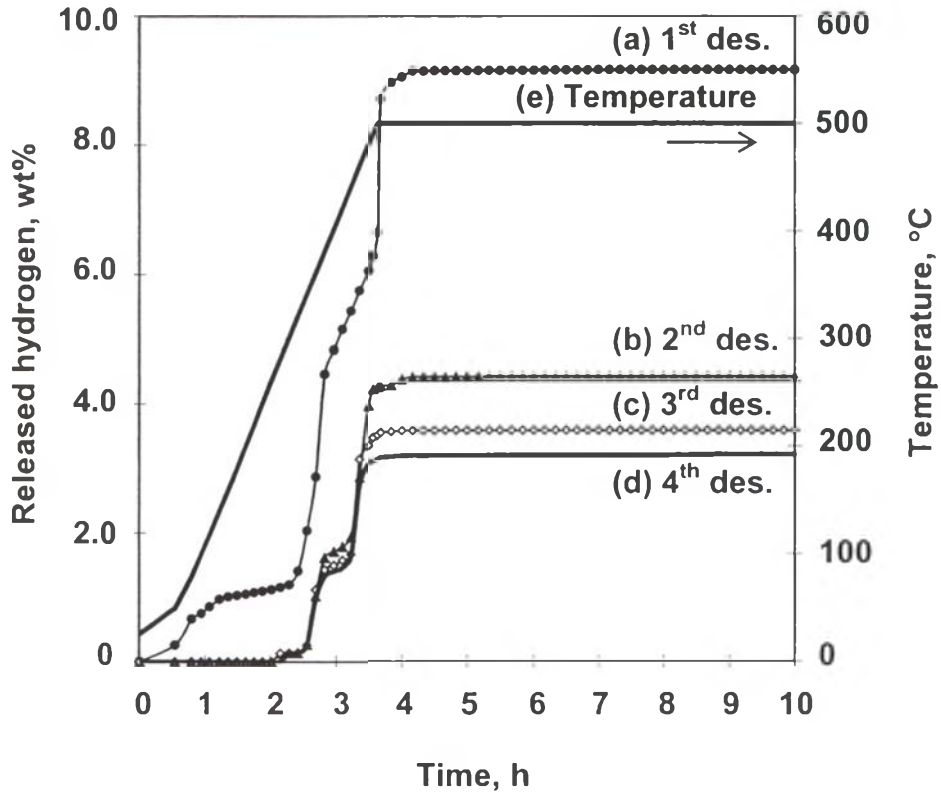

Figure 5.2 Hydrogen desorption profiles of the $LiBH_4/MgH_2$ mixture after ball-milling for 5 h (a) first, (b) second, (c) third, (d) forth hydrogen desorption, and (e) temperature.

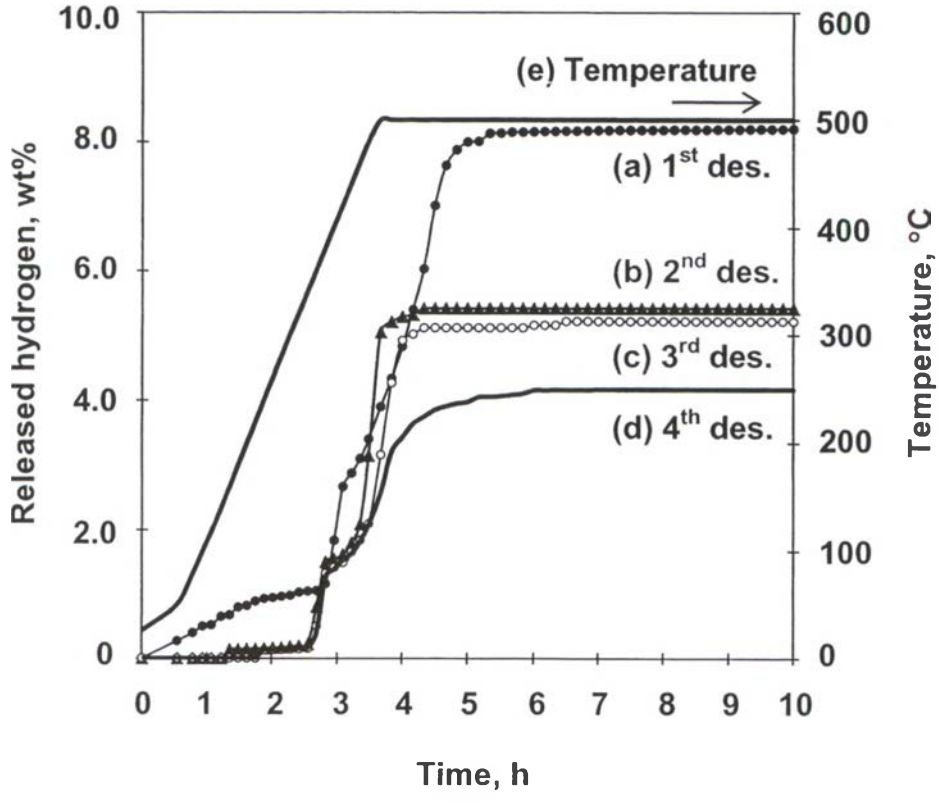

Figure 5.3 Hydrogen desorption profiles of the $LiBH_4/MgH_2$ mixture after ball-milling for 10 h (a) first, (b) second, (c) third, (d) forth hydrogen desorption, and (e) temperature.

Table 5.1 Hydrogen desorption temperature and the total hydrogen capacity of the $LiBH_4/MgH_2$ mixture after ball-milling for 1, 5, and 10 h in the first, second, third, and forth desorption

The $LiBH_4/MgH_2$ mixture	Starting desorption temperature, °C			Cumulative hydrogen capacity, wt%		
	1 h	5 h	10 h	1 h	5 h	10 h
First desorption						
- Step 1	50	50	50	3.0	1.3	1.1
- Step 2	380	330	380	5.4	4.4	2.6
- Step 3	500	380	420	8.6	9.2	8.2
Second desorption						
- Step 1	360	360	340	1.9	1.8	1.5
- Step 2	450	440	420	5.4	4.5	5.4
Third desorption						
- Step 1	360	360	340	1.9	1.8	1.5
- Step 2	450	440	420	3.9	3.6	5.2
Forth desorption						
- Step 1	360	360	340	1.9	1.8	1.5
- Step 2	450	440	420	2.5	3.2	4.2

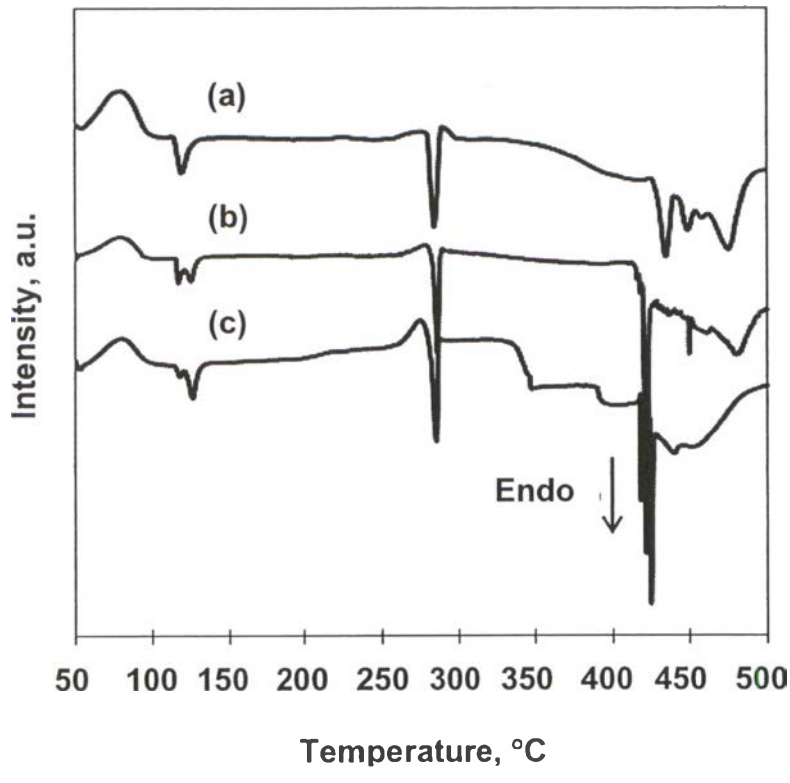

Figure 5.4 DSC patterns of the $LiBH_4/MgH_2$ mixture ball-milled for (a) 1, (b) 5, and (c) 10 h.

In the second step of the first desorption, the samples milled for 1 and 10 h liberate hydrogen at the same temperature of 380°C, while the sample milled for 5 h decomposes at a temperature lower than the other samples about 50°C. The accumulated hydrogen desorption capacity in this step is gradually increased from the first step to 5.4, 4.4, and 2.6 wt% for the samples milled for 1, 5, and 10 h, respectively (Table 5.1). In the third step, the sample with the milling time of 1 h releases hydrogen at 500°C. The desorbed temperature is higher than the other cases, 380°C for 5 h milling time and 420°C for 10 h milling time.

The total hydrogen desorption capacity at 500°C is 8.6, 9.2, and 8.3 wt% for the samples milled for 1, 5, and 10 h, respectively (Table 5.1). The sample milled for 5 h has the highest amount of hydrogen because the Mg phase contained in the starting material reacts with the released hydrogen during the ball-milling process to form more MgH_2 phase. This can be confirmed by the disappearance of the Mg

phase, which was detected in the XRD pattern of the samples after 5 and 10 h ball-milling times (Figs. 5.5(b) and (c), respectively). However, the sample milled for 10 h releases the lowest amount of hydrogen because further increase in the milling time may increase the hydrogen released during the process. All in all, the sample milled for 5 h may be the optimum milling time for the hydrogen desorption/absorption of the $2LiBH_4/MgH_2$ mixture as the sample has the lowest hydrogen desorption temperature and the highest hydrogen desorption capacity in the first desorption.

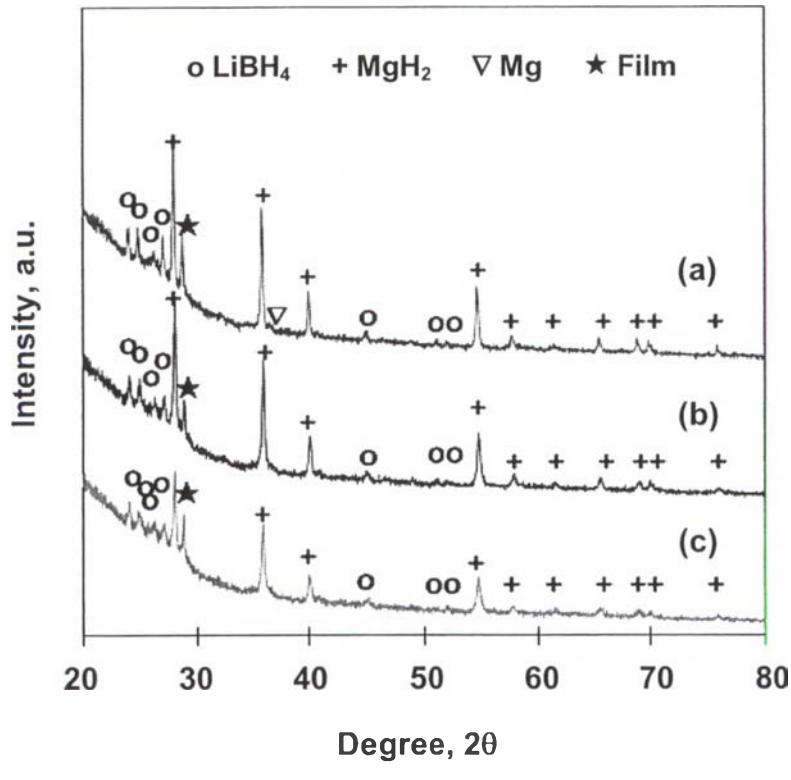

Figure 5.5 XRD patterns of the $LiBH_4/MgH_2$ mixture ball-milled for (a) 1, (b) 5, and (c) 10 h.

The decomposition pathway of the $2LiBH_4/MgH_2$ mixture milled for 5 h (Eqs. (5.1)-(5.6)) can be purposed according to the XRD results of the desorbing hydrogen at various temperatures (Figs. 5.6(a)-(c)).

The decomposition of $LiBH_4$ and MgH_2;

$$LiBH_4 \rightarrow LiBH_{4-X} + \left(\frac{X}{2}\right) H_2 \quad (5.1)$$

$$\rightarrow \left(\frac{1}{12}\right) Li_2B_{12}H_{12} + \left(\frac{10}{12}\right) LiH + \left(\frac{13}{12}\right) H_2 \quad (5.2)$$

$$MgH_2 \rightarrow MgH_{2-Y} + \left(\frac{Y}{2}\right) H_2 \quad (5.3)$$

$$\rightarrow Mg + \left(\frac{2-Y}{2}\right) H_2 \quad (5.4)$$

$$MgH_2 \rightarrow Mg + H_2 \quad (5.5)$$

The reaction between $LiBH_4$ and Mg;

$$2LiBH_4 + Mg \rightarrow 2LiH + MgB_2 + 3H_2 \quad (5.6)$$

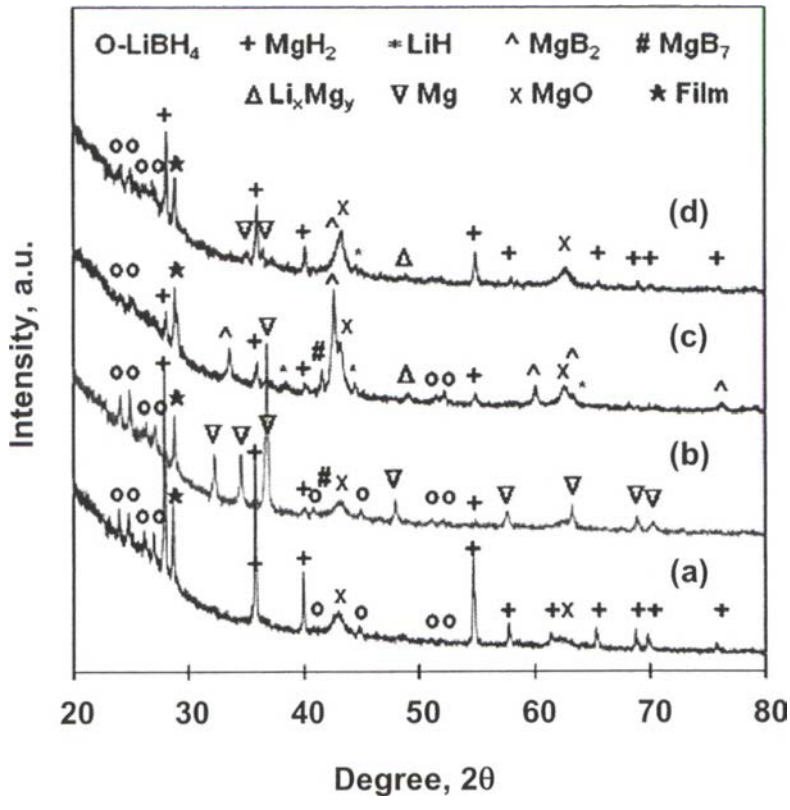

Figure 5.6 XRD patterns of the sample milled for 5 h after hydrogen desorption at (a) 300, (b) 400, (c) 500°C, and (d) after hydrogen absorption.

According to the XRD patterns of the mixture after hydrogen desorption (Figs. 5.6(a)-(c)) and the hydrogen desorption profiles of the sample milled for 5 h (Fig. 5.2), the partial decomposition of the mixture follows Eqs. (5.1)-(5.3), which starts at 50°C. The decomposition of MgH_2 to Mg (Eqs. (5.4)-(5.5)) can be observed at a temperature higher than 380°C because the Mg phase was detected in the XRD pattern at 400°C (Fig. 5.6(b)). The reaction between $LiBH_4$ and Mg (Eq. (6)) takes place at 440°C, which can be confirmed by the presence of LiH and MgB_2 in the XRD pattern at 500°C (Fig. 5.6(c)). It was found that the products after the hydrogen desorption at 500°C are $LiBH_{4-X}$, $Li_2B_{12}H_{12}$, LiH, MgO, MgB_2, MgB_7, Li_XMg_Y, and Mg. The $LiBH_{4-X}$ and $Li_2B_{12}H_{12}$ phases are not detected in the XRD pattern because they have an amorphous structure [24-28]. The MgO phase is the oxide film produced from the reaction between Mg and impurities. The MgB_7 phase is a by-

product between the reaction of rich $LiBH_4$ and MgH_2 [29], while the alloy phase of Li_XMg_Y may be from the reaction between Li and Mg [30]. In addition, the remaining phases of $LiBH_4$ and MgH_2 indicate the incomplete hydrogen.

After completing the hydrogen desorption, the sample was compressed under 8.5 MPa H_2 and 350°C for 12 h in order to absorb hydrogen before the next hydrogen desorption. The absorption reaction follows Eq. (5.7). The phase investigation in Fig. 5.6(d) confirms the recovery of $LiBH_4$ and MgH_2. However, the identification of unconverted MgB_2, Mg, and MgO phases substantiates the incomplete hydrogen absorption of the sample.

$$2LiH + MgB_2 + 4H_2 \rightarrow 2LiBH_4 + MgH_2 \qquad (5.7)$$

For the subsequent hydrogen desorption, Figs. 1-3(b)-(d) show that all three samples release hydrogen in two steps, without the shoulder as observed in the first desorption. This results substantiate the effect of ball-milling process on the partial hydrogen desorption of the hydrides. The decomposition in the first step now starts at 360°C for the sample milled for 1 and 5 h and at 340°C for the sample milled for 10 h. Interestingly, the first step of the desorption releases the same amounts of hydrogen at 1.9, 1.8, and 1.5 wt% for the sample milled for 1, 5, and 10 h, respectively, up to the forth desorption (Table 5.1). In the second step, the sample releases hydrogen at 450, 440, and 420°C for the ball-milling time of 1, 5, and 10 h, respectively. This is consistence with the result from the DSC technique (Fig. 5.4). For the total hydrogen desorption capacity, the samples milled for 1, 5, and 10 h release hydrogen in the range of 2.5-5.4, 3.2-4.5, 4.2-5.4 wt%, respectively, in the second to forth desorption. It clearly shows that the reversibility of the $LiBH_4/MgH_2$ mixture tends to improve with the ball-milling time because the longer the milling time, the more stable the mixture is. A possible reason may be due to better homogeneity between $LiBH_4$ and MgH_2 with the long milling time.

The hydrogen desorption temperature and reversibility enhancement of the $LiBH_4/MgH_2$ mixture can be explained using the XRD results (Fig. 5.5). The figure shows that intensity of the hydride peaks is lower and broader with the increase in

the ball-milling time. It can be deduced that the crystallite size decreases and the lattice strain increases with the prolonged ball-milling time. The results correspond with the calculated crystallite sizes of $LiBH_4$ and MgH_2 from the Scherrer equation [31], as shown in Table 5.2. It has been reported that the defects in the mixture structure can facilitate the hydrogen diffusion in the metal hydride resulting in the lower hydrogen desorption temperature [32-34]. The lower hydrogen desorption temperature and better reversibility of the sample milled for 10 h is a consequence of the lower crystallite size due to the prolonged milling time.

Table 5.2 Crystallite sizes of $LiBH_4$ and MgH_2 after ball-milling for 1, 5, and 10 h

Ball-milling time, h	$LiBH_4$, nm	MgH_2, nm
1	38.79	39.79
5	25.57	37.24
10	23.38	35.57

In addition, the results indicate that the amount of desorbed hydrogen is further reduced after subsequent rehydrogenation. Possible reasons for the decrease are (1) the incomplete hydrogen desorption/absorption, (2) the formation of an amorphous structure during the ball-milling process, $LiBH_{4-X}$ and $Li_2B_{12}H_{12}$, which cannot reverse back to $LiBH_4$, and (3) the formation of MgO, which blocks hydrogen atoms from diffusion into the metal hydride lattice framework and consumes some Mg instead of converting to MgH_2.

5.5 Conclusions

The ball-milling time affects the hydrogen desorption/absorption properties of the $LiBH_4/MgH_2$ mixture with a molar ratio of 2:1. For the first desorption, the samples with different ball-milling times release hydrogen at the same temperature of 50°C. The amount of hydrogen decomposition significantly depends on the ball-

milling process, particularly, in the first step or shoulder. The highest total hydrogen capacity of 9.2 wt% is released from the sample milled for 5 h. For the subsequent hydrogen desorption, the milling time of 10 h exhibits lower hydrogen desorption temperature and better reversibility properties because its hydride crystallite size is smaller than that from the samples milled with other milling times.

5.6 Acknowledgements

This work was supported by National Science and Technology Development Agency (Reverse Brain Drain Project); Royal Jubilee Ph.D. Program (Grant No. PHD/0249/2549), Thailand Research Fund; The Petroleum and Petrochemical College (PPC); Research Unit for Petrochemical and Environment Catalysis, Ratchadapisak Somphot Endowment; the Center of Excellence on Petrochemical and Materials Technology, Thailand; and UOP, A Honeywell Company, USA.

5.7 References

[1] L. Schlapbach, A. Züttel, Nature 414 (2001) 353-358.

[2] A. Züttel, A. Borgschulte, S. Orimo, Scr. Mater. 56 (2007) 823-828.

[3] J.J. Vajo, G.L. Olson, Scr. Mater. 56 (2007) 829-834.

[4] G. Barkhordarian, T. Klassen, M. Dornheim, R. Bormann, J. Alloys Compd. 440 (2007) L18-L21.

[5] G. Barkhordarian, T. Klassen, R. Bormann, Patent pending, German Pub. No: DE102004/061286 (2004).

[6] B. Bogdanović, M. Schwickardi, J. Alloys Compd. 353-254 (1997) 1-9.

[7] G. Liang, J. Huot, S. Boily, A. van Neste, R. Schulz, J. Alloys Compd. 292 (1999) 247.

[8] R. Shulz, J. Huot, G. Liang, S. Boily, G. Lalande, M.C. Denis, Mater. Sci. Eng. A367 (1999) 240.

[9] G. Principi, F. Agresti, A. Maddalena, S.L. Russo, Energy 34 (2009) 2087-2091.

[10] E.M. Fedneva, V.L. Alpatova, V.I. Mikheeva, Russian J. Inorg. Chem. 9 (1964) 826-827.

[11] A. Züttel, S. Rentscha, P. Fischerb, P. Wenger, P. Sudan, Ph. Mauron, Ch. Emmenegger, J. Alloys Compd. 356-357 (2003) 515-520.

[12] A. Züttel, P. Wenger, S. Rentsch, P. Sudan, Ph. Mauron, Ch. Emmenegger, J. Power Sources 118 (2003) 1-7.

[13] M. Au, A. Jurgensen, J. Phys. Chem. B 110 (2006) 7062-7067.

[14] M. Au, A. Jurgensen, K. Zeigler, J. Phys. Chem. B 110 (2006) 26482-26487.

[15] M. Au, A. Jurgensen, W.A. Spencer, D.L. Anton, F.E. Pinkerton, S.-J. Hwang, C. Kim, R.C. Bowman Jr, J. Phys. Chem. C 112 (2008) 18661-18671.

[16] J.J. Vajo, S.L. Skeith, J. Phys. Chem. B 109 (2005) 3719-3722.

[17] M.-Q. Fan, L.-X. Sun, Y. Zhang, F. Xu, J. Zhang, H.-L. Chu, Int. J. Hydrogen Energy 33 (2008) 74-80.

[18] L. Guoxian, W. Erde, F. Shoushi, J. Alloys Compd. 223 (1995) 111-114.

[19] B. Sakintuna, F. Lamari-Darkrim, M. Hirscher, Int. J. Hydrogen Energy 32 (2007) 1123.

[20] H. Gasan, N. Aydinbeyli, O.N. Celik, Y.M. Yaman, J Alloys Compd 487 (2009) 724.

[21] X. Wan, T. Markmaitree, W. Osborn, L.L. Shaw, J. Phys. Chem. C 112 (2008) 18235.

[22] D. Fátay, Ă. Révész, T. Spassov, J. Alloys Compd. 399 (2005) 237.

[23] P. Sridechprasat, Y. Suttisawat, P. Rangsunvigit, B. Kitiyanan, S. Kulprathipanja, Int. J. Hydrogen Energy 36 (2010) 1200-1205.

[24] N. Ohba, K. Miwa, M. Aoki, T. Noritake, S. Towata, Y. Nakamori, S. Orimo, A. Züttel, Phys. Rev. B 74 (2006) 075110.

[25] S. Orimo, Y. Nakamori, N. Ohba, K. Miwa, M. Aoki, S. Towata, A. Züttel, Appl. Phys. Lett. 89 (2006) 021920.

[26] S.-J. Hwang, R.C. Bowman Jr., J.W. Reiter, J. Rijssenbeek, G.L. Soloveichik, J.C. Zhao, H. Kabbour, C.C. Ahn, J. Phys. Chem. C 112 (2008) 3164-3169.

[27] V. Ozolins, E.H. Majzoub, C. Wolverton, J. Am. Chem. Soc. 131 (2009) 230-237.

[28] U. Bösenberg, D.B. Ravnsbæk, H. Hagemann, V.D.'Anna, C.B. Minella, C. Pistidda, W. van Beek, T.R. Jensen, R. Bormann, M. Dornheim, J. Phys. Chem. C 114 (2010) 15212.

[29] S.V. Alapati, J.K. Johnson, D.S. Sholl, J. Phys. Chem. B 110 (2006) 8769-8776.

[30] X.B. Yu, D.M. Grant, G.S. Walker, Chem. Commun. 37 (2006) 3906-3908.

[31] H.P. Klung, L.B. Alexander, X-ray Diffraction Procedures, Wiley, New York, 1974, pp. 687.

[32] J. Huot, G. Liang, S. Boily, A. van Neste, R. Schulz, J. Alloys Compd. 293-295 (1999) 495.

[33] F.C. Gennari, F.J. Castro, G. Urretavizcaya, J. Alloys Compd. 321 (2001) 46.

[34] A. Zaluska, L. Zaluski, J.O. Ström-Olsen, J. Alloys Compd. 288 (1999) 217.